Journal of Catalysis 257 (2008) 32–42

Contents lists available at ScienceDirect

Journal of Catalysis

www.elsevier.com/locate/jcat

# Mechanistic study of propane selective oxidation with $H_2$ and $O_2$ on Au/TS-1

Juan J. Bravo-Suárez [a,1], Kyoko K. Bando [a], Tadahiro Fujitani [a], S. Ted Oyama [a,b,*]

[a] Research Institute for Innovation in Sustainable Chemistry, National Institute of Advanced Industrial Science and Technology, AIST Tsukuba West, 16-1 Onogawa, Tsukuba, Ibaraki 305-8569, Japan

[b] Environmental Catalysis and Nanomaterials Laboratory, Department of Chemical Engineering (0211), Virginia Polytechnic Institute and State University, Blacksburg, VA 24061, USA

ARTICLE INFO

*Article history:*
Received 7 February 2008
Revised 6 April 2008
Accepted 8 April 2008
Available online 20 May 2008

*Keywords:*
Gold
TS-1
Propane
Acetone
2-Propanol
Kinetics
Ultraviolet–visible spectroscopy
X-ray absorption near edge spectroscopy
True intermediate
Oxidation

ABSTRACT

The selective oxidation of propane to acetone and 2-propanol with $H_2$ and $O_2$ was studied on Au/TS-1 by kinetic and spectroscopic analysis. A kinetic study using a factorial design at conditions where the catalyst was stable and gave propane conversions of <6% and combined oxygenates selectivity of >90%, resulted in a power-rate law expression of the form $r_{oxyg.} = k_{oxyg.}(H_2)^{0.74}(O_2)^{0.36}(C_3H_8)^{0.29}$. In situ Au $L_3$-edge X-ray absorption near-edge spectroscopy (XANES) measurements showed activation of $O_2$ on Au, whereas in situ ultraviolet–visible (UV–vis) spectroscopy evidenced the presence of Ti-hydroperoxo species. The role of the Ti-hydroperoxo species was probed by a transient technique in which changes in Ti *K*-edge XANES spectra were used to determine the evolution of coverage with time ($d\theta/dt$). It was shown that the rate of reaction by XANES ($6.7 \times 10^{-4}$ $s^{-1}$) was close to the turnover rate measured in a catalytic flow reactor ($5.6 \times 10^{-4}$ $s^{-1}$), indicating that the hydroperoxo species were true intermediates in the reaction. A proposed reaction sequence in which $H_2O_2$ forms on Au sites and propane is partially oxidized on Ti centers accounts for the spectroscopic results and the reaction orders obtained experimentally for the power-rate law expression.



## 1. Introduction

The discovery that nanometer-sized, highly dispersed supported gold materials can serve as efficient catalysts for several oxidation reactions has stimulated much work in the area [1–3]. In the liquid phase, Au/C catalyzes the epoxidation of *cis*-cyclooctene [4], and Au–Pd/$TiO_2$ catalyzes the oxidation of alcohols to aldehydes [5]. In the gas phase, Au supported on transition metal oxides (e.g., $TiO_2$, $Fe_2O_3$, $Co_2O_3$) has high activity for CO oxidation even at sub-ambient temperatures [1,2,6,7], and Au supported on Ti-containing oxides has high selectivity for propylene epoxidation with $H_2$ and $O_2$ [8,9]. Recently, it has been demonstrated that Au/$TiO_2$ [10] and Au/TS-1 [11] are efficient catalysts for the partial oxidation of propane with $H_2$ and $O_2$. On Au/$TiO_2$, propane is efficiently converted into propylene [10], whereas on Au/TS-1 catalysts, propane is transformed with high selectivity (∼95%) to acetone and 2-propanol [11].

Titanium-substituted silicalite (TS-1) [12] has been shown to catalyze a wide range of selective oxidations, including aromatic hydroxylations, alkane oxidations, and alkene epoxidations, using $H_2O_2$ as the oxidant [13–18]. Compared with alkene epoxidation, the selective oxidation of low-cost abundant alkanes, such as propane, with $H_2O_2$ or $H_2$–$O_2$ mixtures has not been as widely studied. The catalytic oxidation of propane in an autoclave with $H_2O_2$ on TS-1 resulted in oxygenates (acetone and 2-propanol) with high selectivities at a space–time yield (STY) of about 80 $g\,kg_{cat}^{-1}\,h^{-1}$ [14]. The selective oxidation of propane in a flow system with $H_2$–$O_2$ mixtures on Au/TS-1 catalysts has been shown to also produce acetone and 2-propanol at high selectivities (∼95%) with STYs (∼40 $g\,kg_{cat}^{-1}\,h^{-1}$) [11] comparable to those obtained in a batch reactor with $H_2O_2$ [14]. Currently, acetone is formed as a coproduct in the production of phenol by the cumene process [19,20], with a worldwide production of about 5.2 million metric tons in 1999 [21]. There is increasing interest in the direct synthesis of acetone from propane because of the possibility of commercialization of a process for the direct synthesis of phenol from benzene [22–24].

In the liquid phase, propane oxidation with $H_2O_2$ results in the formation of acetone and 2-propanol by attack on the secondary C–H bond of propane. When TS-1 is used as a catalyst, propane activation has been proposed to occur via a 2-propoxy intermediate [13]. In the gas phase, the activation of propane on Au-supported Ti-containing catalysts with $H_2$ and $O_2$ also likely occurs through the formation of a 2-propoxy intermediate species from the reaction of adsorbed propane and $H_2O_2$ produced from

* Corresponding author at: Department of Chemical Engineering (0211), Virginia Polytechnic Institute and State University, Blacksburg, VA 24061, USA. Fax: +1 540 231 5022.
*E-mail address:* oyama@vt.edu (S.T. Oyama).
[1] Present address: Department of Chemical Engineering, University of California, Berkeley, CA 94720, USA.

0021-9517/$ – see front matter 
doi:10.1016/j.jcat.2008.04.004

$H_2$ and $O_2$ on Au [11]. Based on our spectroscopic and kinetic data, here we propose that the likely steps leading to the synthesis of acetone from propane, $H_2$, and $O_2$ involve the following reactions that are known to occur on gold or Ti sites:

- Synthesis of $H_2O_2$ from $H_2$ and $O_2$ on Au nanoparticles [25–27].
- Formation of Ti-hydroperoxo (Ti(OOH)) species from $H_2O_2$ on tetrahedral Ti(OH) sites [28–34].
- Formation of 2-propoxy species from Ti(OOH) and adsorbed $C_3H_8$ [10,11,13].
- Synthesis of acetone from oxidation of 2-propoxy species with $H_2O_2$ [10,11].
- Decomposition of $H_2O_2$ to $H_2O$ [31,32,35].

In this work, the kinetics of propane selective oxidation with $H_2$ and $O_2$ on Au/TS-1 (Ti/Si = 3/100) were also determined. Under certain reaction conditions, acetone and 2-propanol were produced at STYs of about 170 and 15 $g\,kg_{cat}^{-1}\,h^{-1}$, respectively. These results are much higher than those obtained in a batch reactor with expensive $H_2O_2$ [14]. The partial pressure dependence of the rate of formation of acetone on the reactants, $H_2$, $O_2$, and $C_3H_8$ were obtained using a factorial design method, and the resulting kinetics are in agreement with the proposed sequence of steps.

The reaction also was studied in detail with spectroscopic techniques at reaction conditions using a novel transient kinetic analysis. The adsorption of $O_2$ on Au was demonstrated by in situ UV–vis and Au $L_3$-edge XANES spectroscopies, the formation of Ti(OOH) species was investigated by in situ UV–vis spectroscopy, and the Ti(OOH) were identified as true intermediates by a transient Ti *K*-edge XANES spectroscopic technique [34]. The spectroscopic results support the aforementioned sequence of steps. The reaction sequence involves the migration of hydrogen peroxide formed on gold sites to form a reactive hydroperoxide intermediate on Ti sites, and the subsequent reaction of the hydroperoxide species with propane to form a 2-propoxide intermediate that produces oxygenated products [11].

## 2. Experimental

### 2.1. Catalyst preparation

The TS-1 (Ti/Si = 3/100) zeolite support was prepared by the method of Khomane et al. [36] In a typical preparation, 2.0 g of Tween 20 (Aldrich) was dissolved in a solution of 24 g of water (Ultrapure, Wako) and 27.3 g of tetrapropylammonium hydroxide (20–25 wt% aqueous solution; TCI). Then 36.6 g of tetraethylorthosilicate (+95%; Wako) was added dropwise under vigorous stirring. After continuous stirring for 1 h, a clear solution was obtained. A solution of about 1.8 g of tetrabutylorthotitanate (TCI) dissolved in 18 g of 2-propanol (Wako, +99.5%) was added dropwise under vigorous stirring. After another 1 h of stirring, the mixture was transferred to a Teflon-lined autoclave and placed in an oven for hydrothermal crystallization at 433 K for 18 h. The final product was recovered by centrifugation, washed thoroughly with water (Ultrapure, Wako), dried overnight at 383 K, and calcined in air at 813 K ($\sim$2 $K\,min^{-1}$) for 4 h.

The Au supported on TS-1 catalyst was prepared by a deposition–precipitation method. In a typical preparation, 100 ml of a gold solution (3 g of $HAuCl_4{\cdot}4H_2O$ in 1 L of water, $7.2\times10^{-3}$ M) was heated to 343 K under vigorous stirring. The pH of the solution was adjusted to 7.0 within 10 min by addition of 1 M NaOH (Wako, 97.0+%), followed by addition of 1.0 g of TS-1. Stirring was continued for 1 h, after which the suspension was cooled to room temperature. Solids were separated by filtration and washed with 0.3 L of water (Ultrapure, Wako). The solid thus obtained was vacuum-dried overnight at 298 K, and calcined in air at 673 K ($\sim$3 $K\,min^{-1}$) for 3 h.

### 2.2. Catalytic testing

Propane partial oxidation experiments were carried out in a quartz tubular microreactor (6 mm i.d., 180 mm long) using a powder catalyst sample diluted with SiC (Strem) (particle size 63–212 μm; 150 mg of Au/TS-1 and 450 mg of SiC). The empty space before and after the catalyst sample was filled with glass wool to prevent gas-phase reactions. Flow rates of $H_2$ (purity ⩾99.99%, from a hydrogen generator, OPGU-2100S, Shimadzu), $O_2$ (purity ⩾99.5%, Hitachi Sanso), $C_3H_8$ (purity ⩾99.5%, Takachiho Chemical), and Ar (purity ⩾99.9997%, Suzuki Shokan) were regulated by mass flow controllers. The reactor was equipped with an axial quartz thermocouple well (2 mm o.d.), which allowed monitoring of the catalyst bed temperature. Before reaction, the catalyst was pretreated under Ar and held at 443 K for 0.5 h. A typical standard reaction condition used for spectroscopic studies was $H_2/O_2/C_3H_8/Ar = 1/1/1/7$ at a total flow rate of 30 $cm^3\,min^{-1}$, 443 K, and 0.1 MPa (Table 1, run *S*). The space velocity at this standard condition varied from 9000 to 90,000 $cm^3\,h^{-1}\,g_{cat}^{-1}$ as the weight of the catalyst used for UV–vis and XAFS measurements differed. Reaction products were analyzed online using two gas chromatographs (Shimazu GC-14), one equipped with a flame ionization detector (FID) and a thermal conductivity detector (TCD) using a FFAP capillary column (0.32 mm × 60 m) and a Porapak Q packed column (3 mm × 2 m), respectively, and the other equipped with an FID attached to a MS-5A 60/80 packed column (3 mm × 2 m) and TCD attached to a Gaskuropak 54 84/100 packed column (3 mm × 2 m). The FFAP and Porapak Q columns were used to detect oxygenates (e.g., acetaldehyde, propylene oxide, acetone, propionaldehyde, acrolein, acetic acid, and 2-propanol) and $CO_2$ and $H_2O$, respectively, whereas the Gaskuropak 54 84/100 and MS-5A 60/80 columns were used to detect hydrocarbons (e.g., propane, propylene, ethylene, and ethane) and $H_2$, $O_2$, CO, and methane, respectively.

Because the major products observed were acetone ($CH_3COCH_3$), 2-propanol ($CH_3CH(OH)CH_3$), $CO_2$, and $H_2O$, the net reactions occurring on the catalysts were taken as [10]:

$$C_3H_8 + 2H_2 + 2O_2 \rightarrow CH_3COCH_3 + 3H_2O,$$

$$C_3H_8 + H_2 + O_2 \rightarrow CH_3CH(OH)CH_3 + H_2O,$$

$$C_3H_8 + 5O_2 \rightarrow 3CO_2 + 4H_2O,$$

and

$$H_2 + 1/2O_2 \rightarrow H_2O.$$

Based on these reactions, propane conversion, selectivity to $CH_3COCH_3$ and $CH_3CH(OH)CH_3$, and $H_2$ efficiency (selectivity) were defined as follows:

$$\text{Propane conversion} = \frac{\text{mol of (C3 products} + CO_2/3)}{\text{mol of propane in feed}} \times 100,$$

$$\text{C3 product selectivity} = \frac{\text{mol of C3 product}}{\text{mol of (C3 products} + CO_2/3)} \times 100,$$

$$H_2\ \text{efficiency} = \frac{\text{hydrogen consumed by desired reactions}}{\text{total hydrogen consumption}} \times 100$$

$$= \frac{2 \times \text{mol of } CH_3COCH_3 + \text{mol of } CH_3CH(OH)CH_3}{\text{total hydrogen consumption}} \times 100.$$

The kinetic study was carried out at a temperature of 443 K and a total pressure of 0.1 MPa by varying the flow rate of reactants while keeping the total flow rate at 45 $cm^3\,min^{-1}$ by adjusting the flow rate of Ar. The catalyst was stable, and measurements were started after about 7 h of reaction at the initial reaction conditions. A $3^{3-1}$ fractional factorial design methodology was used to obtain

**Table 1**
Summary of catalytic results at different temperatures and with various combinations of reactants following a $3^{3-1}$ fractional factorial design

| Code | Partial pressure (kPa) | | | $C_3H_8$ conv. (%) | Selectivity (%) | | | | $H_2$ eff. (%) | Formation rate (mmol $kg_{cat}^{-1}$ $h^{-1}$) | | | |
|---|---|---|---|---|---|---|---|---|---|---|---|---|---|
| | $H_2$ | $O_2$ | $C_3H_8$ | | Acet. | 2-Pr. | Other | $CO_2$ | | Acet. | 2-Pr. | $CO_2$ | $H_2O$ |
| *S* | 10.1 | 10.1 | 10.1 | 2.0 | 85 | 11 | 0 | 4 | 18 | 842 | 111 | 36 | 10,800 |
| *T*4 | 12.7 | 12.7 | 12.7 | 1.8 | 85 | 7 | 1 | 7 | 10 | 1410 | 116 | 106 | 35,800 |
| *T*1 | 12.7 | 12.7 | 12.7 | 1.0 | 77 | 17 | 3 | 3 | 13 | 681 | 149 | 29 | 10,300 |
| *T*3 | 12.7 | 12.7 | 12.7 | 1.9 | 85 | 10 | 1 | 4 | 13 | 1450 | 177 | 71 | 26,200 |
| *R*0 | 12.7 | 12.7 | 12.7 | 1.6 | 83 | 13 | 0 | 4 | 14 | 1120 | 192 | 50 | 17,300 |
| *R*1 | 12.7 | 12.7 | 12.7 | 1.7 | 85 | 12 | 0 | 3 | 14 | 1320 | 194 | 46 | 21,300 |
| *L*7 | 21.8 | 3.5 | 21.8 | 0.9 | 77 | 19 | 0 | 4 | 9 | 1090 | 273 | 56 | 26,500 |
| *L*5 | 12.7 | 12.7 | 21.8 | 1.2 | 84 | 15 | 0 | 1 | 16 | 1590 | 290 | 24 | 22,600 |
| *L*3 | 3.5 | 21.8 | 21.8 | 0.5 | 75 | 15 | 5 | 5 | 16 | 577 | 114 | 41 | 8070 |
| *L*2 | 3.5 | 12.7 | 12.7 | 0.6 | 80 | 13 | 1 | 6 | 13 | 440 | 73 | 33 | 8000 |
| *L*9 | 21.8 | 21.8 | 12.7 | 3.5 | 90 | 7 | 0 | 3 | 15 | 2900 | 238 | 87 | 46,500 |
| *R*2 | 12.7 | 12.7 | 12.7 | 1.9 | 87 | 11 | 0 | 2 | 15 | 1530 | 187 | 34 | 23,400 |
| *L*8 | 21.8 | 12.7 | 3.5 | 5.2 | 92 | 4 | 0 | 4 | 7 | 1260 | 49 | 59 | 52,500 |
| *L*1 | 3.5 | 3.5 | 3.5 | 1.0 | 93 | 6 | 0 | 1 | 8 | 254 | 18 | 2 | 7460 |
| *L*6 | 12.7 | 21.8 | 3.5 | 4.6 | 92 | 4 | 0 | 4 | 9 | 1120 | 44 | 48 | 32,100 |
| *L*4 | 12.7 | 3.5 | 12.7 | 1.1 | 83 | 13 | 0 | 4 | 10 | 826 | 135 | 39 | 17,700 |
| *R*3 | 12.7 | 12.7 | 12.7 | 1.7 | 83 | 12 | 1 | 4 | 13 | 1280 | 179 | 67 | 21,800 |

*Notes.* Conv.: conversion, Eff.: efficiency, Acet.: acetone, 2-Pr.: 2-propanol. The symbol *S* indicates standard conditions; *L* represents Taguchi orthogonal array elements with numeric labels; *R* denotes repeats; *T* indicates measurements at different temperatures, $T1 = 428$ K, $T3 = 458$ K, $T4 = 473$ K, and the remaining runs at 443 K. Catalyst = 0.52 wt% Au/TS-1 (Ti/Si = 3/100), catalyst weight = 150 mg, total flow rate = 45 $cm^3$ $min^{-1}$ (for standard conditions is 30 $cm^3$ $min^{-1}$), and total pressure = 0.1 MPa.

**Table 2**
Dependencies of formation rates on partial pressure of reactants

| Formation rate | $k$[a] | Dependency | | | | $R^2$ | 95% confidence | | | |
|---|---|---|---|---|---|---|---|---|---|---|
| | | $H_2$ ($l$) | $O_2$ ($m$) | $C_3H_8$ ($n$) | Acetone ($p$) | | $H_2$ ($l$) | $O_2$ ($m$) | $C_3H_8$ ($n$) | Acetone ($p$) |
| Oxygenates | 42.6 | 0.74 | 0.36 | 0.29 | | 0.974 | 0.14 | 0.14 | 0.14 | |
| Acetone | 41.2 | 0.76 | 0.38 | 0.21 | | 0.963 | 0.17 | 0.17 | 0.17 | |
| $CO_2$ | 0.358 | 0.82 | 0.66 | 0.48 | | 0.738 | 0.69 | 0.69 | 0.69 | |
| | $5.21 \times 10^{-8}$ | 3.06 | 1.71 | 0.81 | −2.76 | 0.853 | 2.98 | 1.50 | 0.74 | 3.61 |
| | 66.1 | | 0.33 | 0.37 | 0.87 | 0.647 | | 0.89 | 0.82 | 0.98 |
| $H_2O$ | 1540 | 0.87 | 0.22 | | | 0.951 | 0.18 | 0.18 | | |
| | 2330 | 0.88 | 0.22 | −0.18 | | 0.989 | 0.095 | 0.095 | 0.095 | |
| | 2150 | 0.89 | 0.23 | −0.18 | −0.014 | 0.989 | 0.54 | 0.27 | 0.14 | 0.66 |

[a] Units will vary so that the formation rate is given in mmol $kg_{cat}^{-1}$ $h^{-1}$. Catalyst = 0.52 wt% Au/TS-1 (Ti/Si = 3/100), catalyst weight = 150 mg, total flow rate = 45 $cm^3$ $min^{-1}$, $H_2$, $O_2$, and $C_3H_8$ partial pressure range = 3.5–21.8 kPa, temperature = 443 K, and total pressure = 0.1 MPa.

rate parameters over a fairly large range of reactant partial pressures [37]. Three levels of partial pressure—3.5, 12.7, and 21.8 kPa—were used for each reactant, $H_2$, $O_2$, and $C_3H_8$. The partial pressure combinations were set such that they followed a Taguchi orthogonal array *L*9 (*L*1 to *L*9 in Table 1). Measurements at the central level ($H_2/O_2/C_3H_8$ = 12.7/12.7/12.7 kPa) were also carried out at other temperatures ($T1 = 428$ K, $R = 443$ K, $T3 = 458$ K, and $T4 = 473$ K). Each measurement was taken after stable rates were achieved, which took about 1 h. The order of the experiments was varied randomly, and the experiments were carried out sequentially as shown in the first column of Table 1. The highest temperature point was measured first, to minimize possible catalyst changes. The first entry (run *S*) of Table 1 is typical of in situ spectroscopic experiments, entries 2–5 are used for the estimation of activation energies, and entries 7–16 are used to fit the studied models. Despite the limited number of experimental data points (10), sufficient points are available to obtain relevant results as the number of degrees of freedom, data points ($N$) minus model parameters ($p$), is positive and >5 [32]. To verify the lack of catalyst deactivation, runs at the central level at 443 K (*R*0) were repeated during and after the experiments (*R*1, *R*2, and *R*3). Power-rate law expressions (Table 2) were obtained by simultaneously fitting the logarithms of the partial pressures (kPa) of each reactant and the formation rate (mmol $kg_{cat}^{-1}$ $h^{-1}$) data by linear least squares regression analysis using the POLYMATH 5.1 program [38]. Internal mass transfer limitations were neglected, because the Weisz–Prater parameter (CWP) was estimated to be $5 \times 10^{-4} < 1$ [39].

### 2.3. Characterization

Transmission electron microscopy (TEM) images were obtained in a microscope (UT-Philips CM200) operated at 200 kV. In situ UV–vis spectra were collected under reaction conditions using a large-compartment spectrometer (Varian Cary 5000) equipped with a Harrick Scientific reaction chamber (model HVC-DRP) and a praying mantis diffuse reflectance attachment (DRP-XXX). Powder catalyst (~50 mg) was loaded into the reaction chamber, the temperature of which was monitored by a thermocouple added to the Harrick cell just under the center of the sample. Reaction conditions (e.g., temperature, pressure, gas flow rates) were the same as for the reactivity measurements (Table 1, run *S*). Spectra were referenced to the same material under Ar just before the start of the reaction (difference spectra) or to $BaSO_4$. Diffuse reflectance spectra were analyzed using the Kubelka–Munk function, $F(R_\alpha)$, calculated from absorbance data [40]. In situ Au $L_3$-edge X-ray absorption fine structure (XAFS) measurements under propane partial oxidation conditions ($H_2/O_2/C_3H_8/He$ = 1/1/1/7, 443 K, 0.1 MPa) were carried out at beamline BL9A of the Photon Factory in the Institute of Materials Structure Science, High-Energy Accelerator

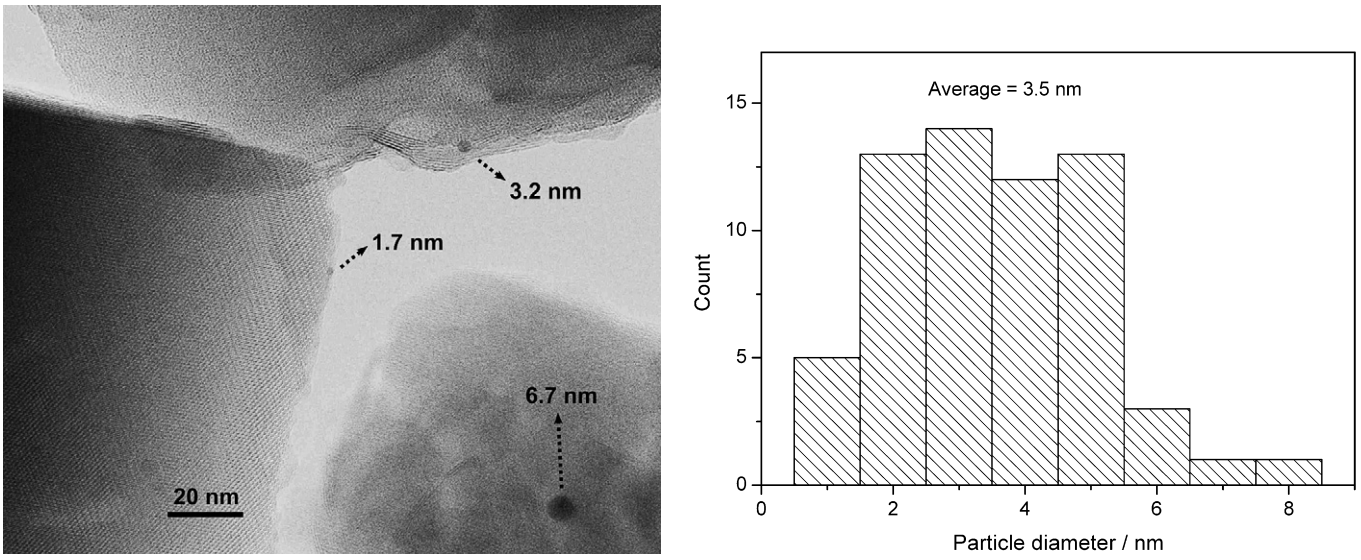


**Fig. 1.** TEM micrograph and particle size distribution of Au/TS-1 catalyst.

Research Organization (PF-IMSS-KEK) in Tsukuba, Japan. In situ Ti *K*-edge XAFS measurements were also carried out at two different reaction conditions, one in the presence of $H_2$ and $O_2$ ($H_2/O_2$/He = 1/1/8, 443 K, 0.1 MPa) and the other in the presence of $H_2$, $O_2$, and $C_3H_8$, ($H_2/O_2/C_3H_8$/He = 1/1/1/7, 443 K, 0.1 MPa). Ti *K*-edge XAFS spectra were obtained every 150 s in a step-scanning mode using the same pretreatment and reaction conditions as used in the catalytic testing reactor (Table 1, run *S*), but with He as the inert gas. All spectra were obtained in transmission mode using an in situ XAFS cell provided with a flow delivery system. Sample wafers (diameter = 1 cm) were prepared from 200 mg of catalyst for Au $L_3$-edge measurements and 20 mg of catalyst for Ti-edge XAFS measurements. Pretreatment and reaction conditions were monitored and controlled from outside the radiation shield hutch. Gold content in the catalyst was estimated from the Au $L_3$-edge XAFS edge-jump absorption intensity by comparison with a gold-supported TS-1 sample of known Au concentration. XAFS data were analyzed with commercially available software (REX, Rigaku Co.).

## 3. Results

The catalyst used in this study comprised nanometer-sized gold particles highly dispersed on a microporous titanosilicate, TS-1 (Ti/Si = 3/100), prepared by deposition-precipitation at a pH of 7 using NaOH as the neutralizing agent. Au $L_3$-edge XAFS measurements of the Au/TS-1 catalyst indicated that it had a gold loading of 0.52 wt%, and a Au coordination number (CN) of 10.4, corresponding to a particle size ($D_p$) of 3.4 nm assuming Au fcc packing and spherical particles. The error introduced by estimating the Au content of the catalyst (0.52 wt%) from the Au $L_3$-edge XAFS edge-jump absorption intensity would be expected to be small in comparison with a reference sample, a gold supported TS-1 of similar composition and gold content (0.11 wt%). The nominal Ti content for this catalyst with a Ti/Si ratio of 3/100 is estimated as 477 μmol $g_{cat}^{-1}$. Fig. 1 presents a high-resolution TEM image of the Au/TS-1 catalyst and its particle size distribution, which was centered at 3.5 nm. Gold particles with a diameter of 3.5 nm exhibited a dispersion of about 40%, resulting in an exposed gold content of 10.6 μmol $g_{cat}^{-1}$.

Table 1 gives the factorial design used for the kinetic study with the Au/TS-1 catalyst, comprising 10 runs with various combinations of reactant partial pressures at a temperature of 443 K and a

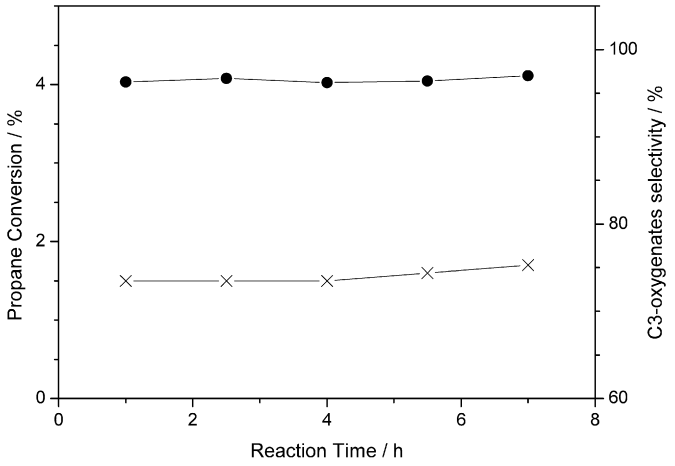


**Fig. 2.** Propane conversion and C3-oxygenates selectivity over Au/TS-1 catalyst with reaction time on stream. Reaction conditions: $H_2/O_2/C_3H_8$/Ar = 5.6/5.6/5.6/26.8 $cm^3\,min^{-1}$. Space velocity = 18,000 $cm^3\,h^{-1}\,g_{cat}^{-1}$, $T = 443$ K, $P = 0.1$ MPa.

total pressure of 0.1 MPa. The data were obtained at propane conversions <6% and C3-oxygenates selectivity >90%. Propane conversion increased with $H_2$ and $O_2$ partial pressures but appeared to decrease with propane partial pressure. The C3-oxygenates combined selectivity remained high (>90%) during the experimental study. Acetone was the main product, with selectivities >75%, whereas 2-propanol selectivities reached values as high as ca. 20%. Here the rates are expressed in mmol $kg_{cat}^{-1}\,h^{-1}$, but they can be converted to turnover frequencies (TOF; $s^{-1}$) by the conversion factor (1/*S*) (1/3600), where *S* is the surface gold (10.6 μmol $g_{cat}^{-1}$) or titania (477 μmol $g_{cat}^{-1}$) content. The formation rate of oxygenates (acetone and 2-propanol) did not track with propane conversion, because different inlet propane partial pressures were used. In general, oxygenates formation rate increased with $H_2$, $O_2$, and $C_3H_8$ partial pressures (see Supporting Information). Hydrogen efficiency (selectivity to oxygenates) varied depending on the reaction conditions, but appeared to increase at low $H_2$, high $O_2$, and high $C_3H_8$ partial pressures (runs *L1*, *L2*, and *L3*). Under reaction conditions typical of in situ spectroscopy experiments (Table 1, run *S*), at steady state, propane conversion was 2% with a selectivity to oxygenates (acetone and 2-propanol) of 96%, resulting in an STY of 56 g $kg_{cat}^{-1}\,h^{-1}$. The steady-state oxygenates turnover rate based on

surface gold atoms was $2.5 \times 10^{-2}\,s^{-1}$, and that based on total Ti was $5.6 \times 10^{-4}\,s^{-1}$.

Fig. 2 shows the reactivity over the Au/TS-1 catalyst as a function of reaction time. Propane conversion and oxygenates (acetone and 2-propanol) selectivity remained relatively stable for up to 7 h. The catalyst also remained stable during the course of the kinetic study, as verified by repetition of the central level run at the beginning, during, and at the end of the experiments (Table 1, runs *R*0, *R*1, *R*2, and *R*3).

Table 2 presents the dependence of the formation rates of C3-oxygenates, acetone, $CO_2$, and $H_2O$ on the nominal inlet partial pressures of $H_2$, $O_2$, and $C_3H_8$ as a power rate law expression $r = k(H_2)^l(O_2)^m(C_3H_8)^n$. Water was found to have little effect on the formation rates when introduced in the feed as a vapor (2.2%), and thus it was not considered in the model fits. The best fits for the C3-oxygenates, acetone, and $H_2O$ were

$$r_{\text{oxyg.}} = k_{\text{oxyg.}}(H_2)^{0.74}(O_2)^{0.36}(C_3H_8)^{0.29},$$

$$r_{\text{acet.}} = k_{\text{acet.}}(H_2)^{0.76}(O_2)^{0.38}(C_3H_8)^{0.21},$$

and

$$r_{\text{water}} = k_{\text{water}}(H_2)^{0.89}(O_2)^{0.23}(C_3H_8)^{-0.18}.$$

The overall models fits were relatively good, with $R^2$ values >0.960. The oxygenates formation rate depended mainly on $H_2$ partial pressure, and also on $O_2$ and $C_3H_8$ partial pressures.

Fig. 3 presents power-rate law model parity plots and residuals of the formation rates of $H_2O$, $CO_2$, and oxygenates. The parity plot lines pass through the origin and show no systematic deviations. The residual plots, expressed as a percentage of the experimental rate, show that the errors in the data are randomly distributed. Fig. 4 shows Arrhenius plots for the formation rates of $H_2O$, acetone, and $CO_2$, which yielded corresponding activation energies of 42, 38, and 40 kJ mol$^{-1}$.

The in situ UV–vis spectra of Au/TS-1 under reaction conditions as a function of time exhibited bands characteristic of the gold nanoparticles and the TS-1 support (see Supporting Information). A broad band at around 520 nm (2.38 eV) was due to a plasmon resonance of the gold nanoparticles, whereas the bands at 240 nm (5.17 eV) and 350 nm (3.54 eV) can be assigned to tripodal Ti-hydroperoxo species (Ti(OOH)) or tripodal hydroxo Ti (Ti(OH)(OSi)$_3$), and hydrated Ti-hydroperoxo species (Ti(OOH)), respectively [11,41]. Fig. 5 shows the gold plasmon resonance (PR) position changes during in situ UV–vis measurements under reaction conditions on the Au/TS-1 catalyst as a function of time. The PR position showed an initial increase (red shift) during the first 0.5 h, followed by a decrease (blue shift), reaching a constant value of 520.3 nm after 2–3 h of reaction. The initial red shift is assigned to adsorption of $O_2$ on the gold nanoparticles (Au–O species) [42,43], whereas the blue shift is explained by the partial reduction of these Au–O species, likely with $H_2$ present in the reactant gas. The PR position under reductive $H_2$ flow ($H_2$/Ar, 10 vol%) measured after reaction was 516.0 nm.

Fig. 6 shows the in situ difference spectra for the Au/TS-1 catalyst under reaction conditions as a function of time. As can be seen, three main bands evolved with reaction time: a band at 237 nm (5.23 eV) due to tripodal Ti hydroperoxo sites (Ti(OOH)(OSi)$_3$); a shoulder at around 272 nm (4.56 eV), assigned to hydrated tripodal Ti tetrahedral sites (Ti(OH)(H$_2$O)$_2$(OSi)$_3$); and a broad band centered at around 355 nm (3.49 eV) assigned to hydrated Ti-hydroperoxo species (Ti(OOH)(H$_2$O)$_2$) [11,33,41].

Fig. 7 presents the in situ Au $L_3$-edge XANES spectra, normalized to the same edge jump, for Au/TS-1 under reaction conditions. The catalyst spectra show three near-edge features at 11,935, 11,949, and 11,970 eV, which are characteristic of metallic gold. No cationic gold was observed during reaction conditions, as indicated by the absence of a near-edge resonance around 11,920 eV similar to that observed in a $HAuCl_4$ reference sample. Fig. 8 presents the in situ Au $L_3$-edge XANES difference spectra $\mu$(Reaction) – $\mu$(He, at 443 K before reaction), clearly showing that a transient resonance centered at about 11,921 eV developed in the initial stages of the reaction. It initially grew during the first 0.1 h of reaction, but then decreased, reaching a relative stable value after 1.0–1.5 h of reaction. The feature can be related to the formation of Au–O species by interaction of gold with adsorbed oxygen [44,45], whereas the decrease indicates that the Au–O complex was reduced under reaction conditions.

Fig. 9 shows the in situ Ti *K*-edge XANES spectra for the Au/TS-1 catalyst under reaction conditions ($H_2/O_2/C_3H_8$/He = 1/1/1/7) as a function of time. The spectra present a Ti pre-edge peak centered at 4969.0 eV that decreased with reaction time. This pre-edge feature is characteristic of fourfold-coordinated Ti sites [46,47]. The fractional decrease in the Ti pre-edge peak area from its value before the introduction of the reactants is defined as the coverage, $\theta$, on the Ti centers. The decrease in the pre-edge area is a direct result of an increase in the coordination of Ti. Fig. 10 shows the increased coverage on Ti during the first 450 s of reaction with $H_2/O_2$/He (1/1/8) and $H_2/O_2/C_3H_8$/He (1/1/1/7). The initial rate of increase of coverage was faster with $H_2/O_2$/He than with $H_2/O_2/C_3H_8$/He. The slopes at time zero for the $H_2/O_2$/He and $H_2/O_2/C_3H_8$/He transient curves were $7.4 \times 10^{-4}$ and $7.3 \times 10^{-5}\ s^{-1}$, respectively.

## 4. Discussion

The catalyst used in this work, Au/TS-1, consisted of gold nanoparticles deposited on a microporous titanosilicate (TS-1; Ti/Si = 3/100) support [12,17,41,48]. The gold content in the catalyst of 0.52 wt% corresponded to gold nanoparticles with an average particle size of 3.5 nm as estimated from TEM measurements (Fig. 1). This result is in excellent agreement with the particle size of 3.4 nm estimated from Au $L_3$-edge XAFS measurements. The ca. 40% dispersion for this size Au particle corresponds to an exposed Au content of 10.6 μmol $g_{cat}^{-1}$.

Propane selective oxidation with $H_2$ and $O_2$ on the Au/TS-1 catalyst was stable (Fig. 2), enabling the kinetic measurements described in this study (Table 1). Under the standard reaction conditions typical of the in situ spectroscopic measurements (Table 1, run *S*), propane conversion was 2% and oxygenates (acetone and 2-propanol) selectivity was 96%. From these values, the oxygenates TOF was calculated as $5.6 \times 10^{-4}\ s^{-1}$ based on total Ti and $2.5 \times 10^{-2}\ s^{-1}$ based on surface gold atoms. The TOF based on Ti was lower than on Au, because the catalyst contained about 50 times more Ti atoms (477 μmol $g_{cat}^{-1}$) than surface gold atoms (10.6 μmol $g_{cat}^{-1}$). It has recently been shown that TOF also can be measured independently by appropriate in situ spectroscopic techniques for reacting species by transient measurements of coverage versus time ($d\theta/dt$) [34]. If the TOF of the reacting species measured spectroscopically is of similar magnitude to the TOF measured in the conventional reactor, then the reacting species can be considered a true intermediate [34,49–51]. In the present study, we demonstrated this property for the hydroperoxide species on the Ti sites through in situ XAFS spectroscopy measurements, as discussed later in more detail.

The maximum rate of oxygenates (acetone and 2-propanol) formation on the Au/TS-1 catalyst was 3140 mmol $kg_{cat}^{-1}\,h^{-1}$, corresponding to 183 g $kg_{cat}^{-1}\,h^{-1}$ (Table 1, run *L*9). This value is much higher than the values previously reported in the literature for similar catalysts for propane oxidation with reduced activated $O_2$ or $H_2O_2$; for instance, a Au/$TiO_2$/$SiO_2$ catalyst using $H_2$ and $O_2$ oxidized propane to produce acetone (∼50%) at a STY of < 1 g $kg_{cat}^{-1}\,h^{-1}$ [8]; a $H_2$–$O_2$ cell system provided with

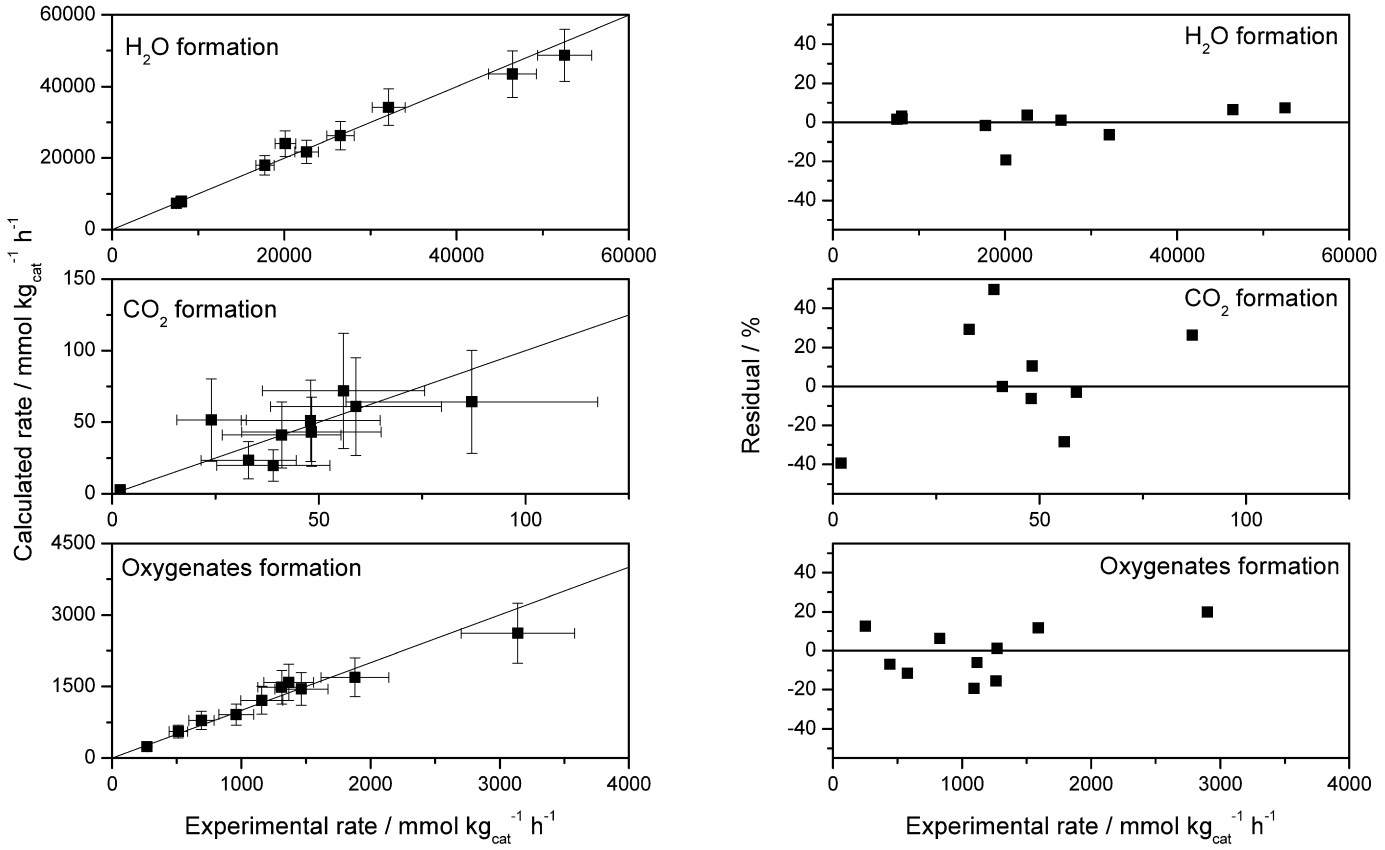


**Fig. 3.** Parity plots and residuals of the calculated and experimental oxygenates, $CO_2$, and $H_2O$ formation rates.

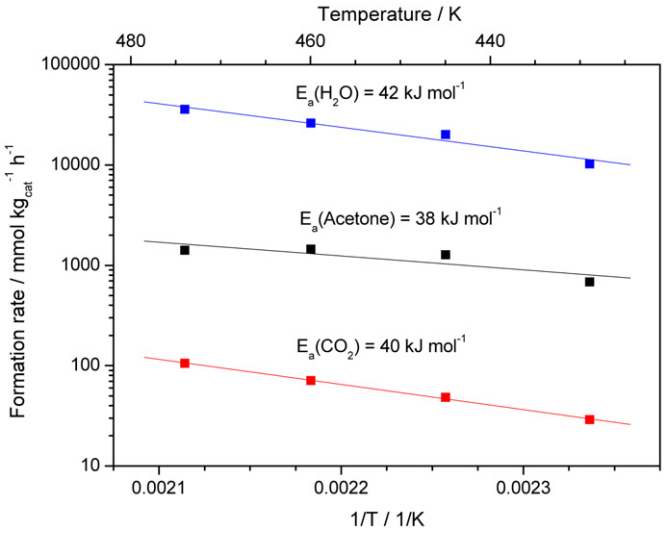


**Fig. 4.** Arrhenius plots of formation rates of $CO_2$, acetone, and $H_2O$.

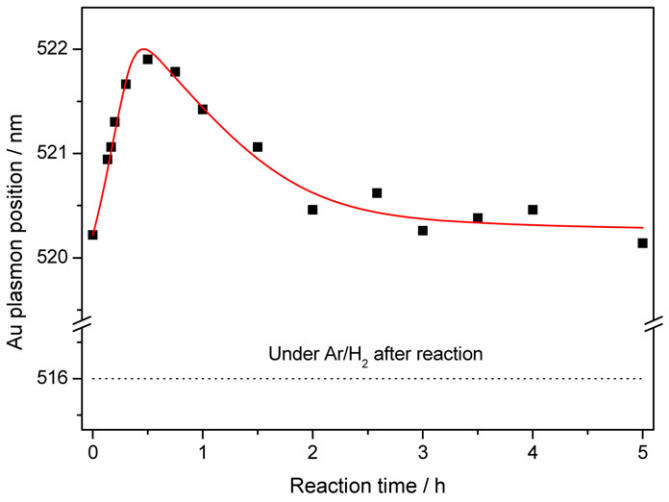


**Fig. 5.** In situ Au plasmon resonance position for Au/TS-1 catalyst under reaction conditions as a function of time.

a Pd + VO(acac)$_2$/VGCF cathode oxidized propane to form acetone (39%) and acetaldehyde (13%) at a STY of 6 $g\,kg_{cat}^{-1}\,h^{-1}$ [52]; a three-phase reactor using a catalytic hollow fiber membrane (HF15/Nafion/PEEK-WC) and the Fenton system, $Fe^{2+}$–$H_2O_2$, carried out the propane oxidation to oxygenates (96%; acetone, 2-propanol, 1-propanol, and propionic aldehyde) at a STY of 5 $g\,kg_{membrane}^{-1}\,h^{-1}$ [53]; and a batch reactor using TS-1 and expensive $H_2O_2$ produced oxygenates (~100%; acetone and 2-propanol) at a STY of 79 $g\,kg_{cat}^{-1}\,h^{-1}$ [14]. Table 1 also summarizes the reaction rate results for different partial pressures of reactants used to determine the kinetics of propane oxidation on Au/TS-1. Propane conversion was <6%, the selectivity to C3-oxygenates was >90%, and the $H_2$ efficiency varied between about 5 and 20%. It should be noted that these results are similar to those for propylene epoxidation to propylene oxide (PO) on gold-supported catalysts at low temperature (<473 K) which presented propylene conversions as high as 8%, PO selectivities >90%, and $H_2$ efficiencies <40% [28–32].

From Table 1, it can be seen that the rate of C3-oxygenates formation was increased by simultaneously increasing the partial pressures of $H_2$, $O_2$, and $C_3H_8$ (run *L*1, $H_2/O_2/C_3H_8 = 3.5/3.5/3.5$, and run *R*, $H_2/O_2/C_3H_8 = 12.7/12.7/12.7$). The partial pressures of

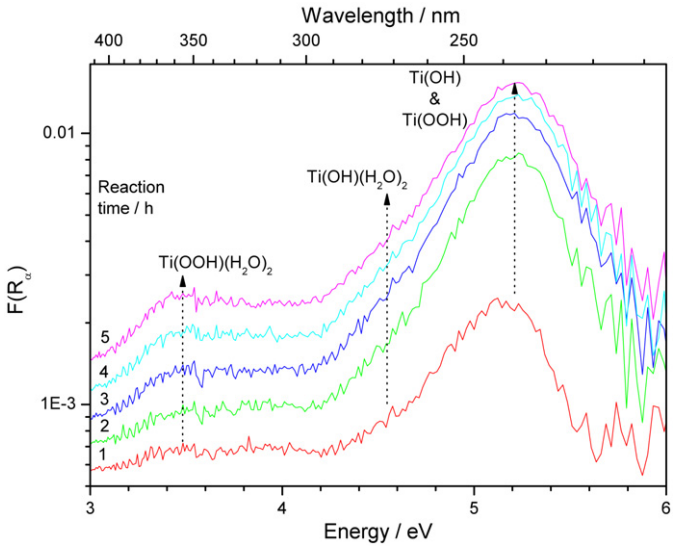


**Fig. 6.** In situ UV–vis difference spectra for Au/TS-1 catalyst under reaction conditions as a function of time. Spectra referenced to catalyst before reaction in Ar (difference spectra).

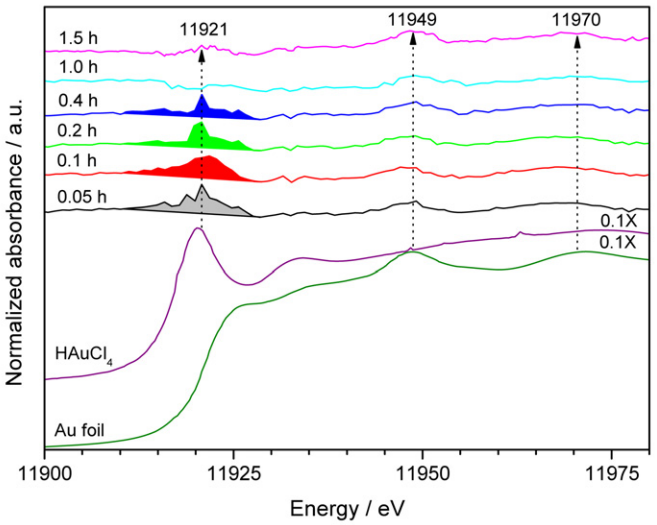


**Fig. 8.** In situ Au $L_3$-edge XANES difference spectra, $\mu$(Reaction) − $\mu$(He) at 443 K before reaction, for Au/TS-1 under propane selective oxidation conditions as a function of reaction time.

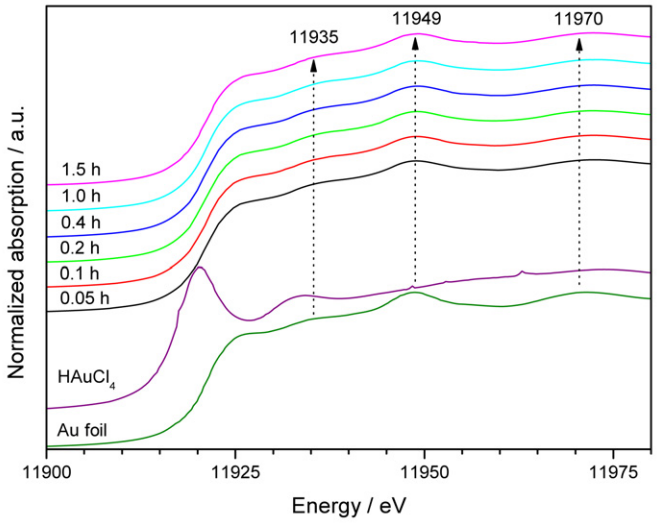


**Fig. 7.** In situ Au $L_3$-edge XANES for Au/TS-1 under propane selective oxidation conditions as a function of reaction time.

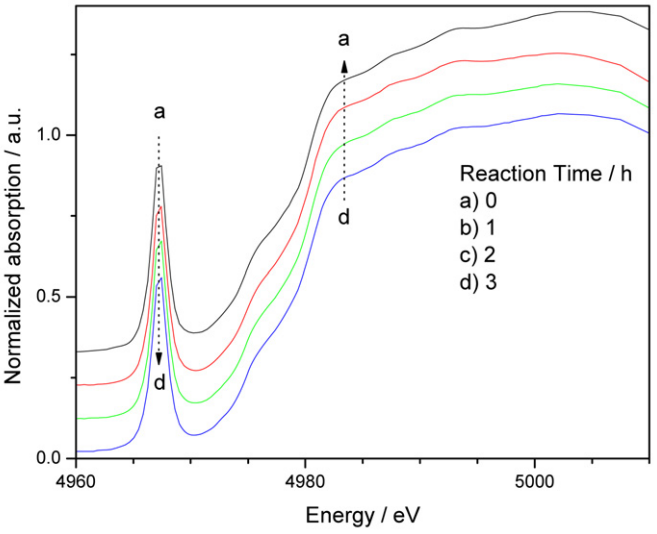


**Fig. 9.** In situ Ti $K$-edge XANES spectroscopy results for Au/TS-1 under propane selective oxidation conditions as a function of reaction time.

$H_2$ and $O_2$ had particularly strong effects on C3-oxygenates formation; for example, the lowest oxygenates STY (272 mmol $kg_{cat}^{-1}$ $h^{-1}$) occurred at low $H_2$ and $O_2$ partial pressures (run *L*1, $H_2/O_2/C_3H_8$ = 3.5/3.5/3.5), whereas the largest STY (3140 mmol $kg_{cat}^{-1}$ $h^{-1}$) was obtained at high $H_2$ and $O_2$ partial pressures (run *L*9, $H_2/O_2/C_3H_8$ = 12.7/21.8/21.8); see Supporting Information.

These results suggest that both $H_2$ and $O_2$ may be involved in the formation of a reaction intermediate, such as a hydroperoxide species [33,54]. This species has been detected on a Au/$TiO_2$ catalyst by inelastic neutron scattering (INS) experiments (at 20 K) after reaction with flowing $H_2/O_2$ at 423 K [55]; on a Pd/TS-1 catalyst by means of EPR and UV–vis spectroscopy after contact with $H_2$, followed by $O_2$ at 323–343 K [56]; on a Au/(mesoporous)Ti–$SiO_2$ by EPR after gas-phase reaction with $H_2$ and $O_2$ at 423 K; by in situ UV–vis [33]; and on a Au–Ba/Ti-TUD by in situ UV–vis and XAFS spectroscopy under reaction conditions with $H_2$ and $O_2$ [34].

Table 2 gives the dependencies of formation rates on the partial pressure of reactants as calculated from regression analysis. Power-rate law fitting for oxygenates, acetone, and $H_2O$ formation rates exhibited $R^2$ values >0.96, with the fitting for $CO_2$ formation rates not as good. This was because of the relatively large variance of the experimental error (Fig. 3), probably due to the low sensitivity in the analytical system at the rather low $CO_2$ selectivities (<6%) obtained in this study. Consequently, we do not discuss $CO_2$ formation models any further in this paper. Fig. 3 presents parity plots and residuals between measured and calculated values. An apparent increasing trend for the residuals at the highest level of oxygenates formation can be explained by the limited number of experimental points under such conditions. For the rate of oxygenates formation, the dependencies on $H_2$, $O_2$, and $C_3H_8$ were 0.74, 0.36, and 0.29, respectively (Table 2). Similar dependencies were obtained for acetone formation (0.76, 0.38, and 0.21, respectively), the main oxygenate product. These positive fractional dependencies orders indicate that $H_2$, $O_2$, and $C_3H_8$ were adsorbed on the surface of the catalyst, but not necessarily on the same sites [32,57,58]. Additionally, they indicate that the adsorbed species should be involved in steps that determine the formation rate [57,58]. We provide a more detailed discussion

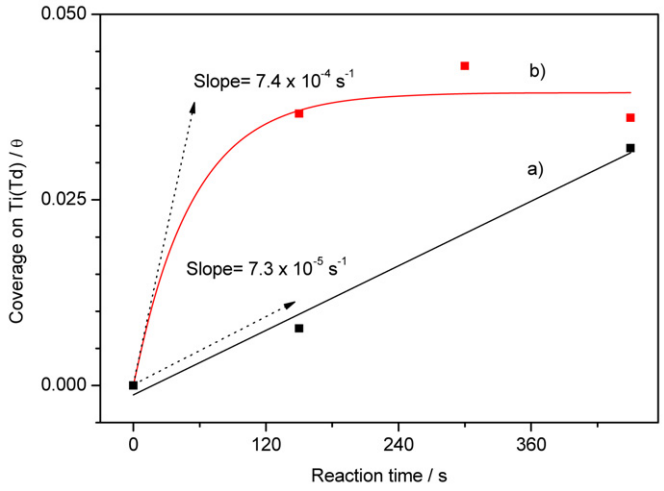


**Fig. 10.** Coverage on 4-fold coordinated Ti ($\theta$, fractional decrease of pre-edge peak area in the Ti *K*-edge XANES spectra) for Au/TS-1 under (a) $H_2/O_2/C_3H_8/He = 1/1/1/7$ (bottom) and (b) $H_2/O_2/He = 1/1/8$ (top) at 443 K and 0.1 MPa during the first 450 s of reaction.

of a possible sequence of steps during propane oxidation, including $H_2$, $O_2$, and $C_3H_8$ species later in this section. For the rate of $H_2O$ formation, the respective dependencies on $H_2$, $O_2$, and $C_3H_8$ were 0.88, 0.22, and −0.18 (Table 2). The positive fractional exponents indicate that $H_2O$ was formed mainly by reaction of $H_2$ and $O_2$, whereas the negative fractional exponent suggests that propane was detrimental for this reaction, probably because it captures some of the $H_2O_2$ that otherwise would decompose to $H_2O$. The exponent values of $H_2$ and $O_2$ (0.88 and 0.22, respectively) are consistent with those reported previously for $H_2$ oxidation on a 0.15 wt% Au on TS-1 (1 wt% Ti) catalyst (0.76 and 0.17, respectively) [35]. The dependency of $H_2O$ production on the acetone partial pressure was found to be −0.014. This small value indicates a quite small contribution of propane partial oxidation to water formation in comparison with the oxidation of $H_2$.

The Arrhenius plots for the formation of $H_2O$, acetone, and $CO_2$ produce apparent activation energies of 42, 38, and 40 kJ mol$^{-1}$, respectively (Fig. 4). The apparent activation energy for $H_2O$ formation (42 kJ mol$^{-1}$) is in good agreement with the value of 37 kJ mol$^{-1}$ reported for $H_2$ oxidation on a 0.15 wt% Au on TS-1 (1 wt% Ti) [35] and with the values of 38–42 kJ mol$^{-1}$ for $H_2$ oxidation on $Au/TiO_2$ [59]. The apparent activation energy for $C_3H_8$ partial oxidation to acetone of 38 kJ mol$^{-1}$ agrees well with the values of 43–48 kJ mol$^{-1}$ for $C_3H_8$ total combustion on $Au/TiO_2$ catalysts [59]. Similar values have been obtained for propylene epoxidation with $H_2$ and $O_2$ on Au–Ba/Ti-TUD (43 kJ mol$^{-1}$) [31], Au/TS-1 (35 kJ mol$^{-1}$) [60], and $Au/TiO_2$ (47 kJ mol$^{-1}$) [61]. The apparent activation energy for $CO_2$ (40 kJ mol$^{-1}$), although smaller than that determined during propylene epoxidation on Au–Ba/Ti-TUD (80 kJ mol$^{-1}$) [31], falls within the energy range for CO oxidation on $Au/TiO_2$ catalysts of 25–72 kJ mol$^{-1}$ [59].

Further discussion on the kinetics of propane selective oxidation with $H_2$ and $O_2$ requires knowledge of the reaction mechanism. Although little is known about this reaction on Au catalysts, the similarities in the reaction orders of propane partial oxidation using $H_2$ and $O_2$ ($r_{oxyg.} = k_{oxyg.}(H_2)^{0.74}(O_2)^{0.36}(C_3H_8)^{0.29}$) with those for $H_2$ oxidation ($r_{H_2O} = k_{H_2O}(H_2)^{0.76}(O_2)^{0.17}$) [35] and propylene epoxidation with $H_2$ and $O_2$ on Au/TS-1 ($r_{PO} = k_{PO}(H_2)^{0.60}(O_2)^{0.31}(C_3H_8)^{0.18}$) [60] suggest a possibly similar sequence of steps. Recently, reaction pathways for $H_2$ oxidation and propylene epoxidation to propylene oxide using $H_2$ and $O_2$ with Au supported on Ti-containing catalysts have been proposed [31,34,35,60].

The reaction rate for propylene oxide formation appears to be determined by two irreversible steps: the production of $H_2O_2$ on a Au site and the oxidation of the propylene by a hydroperoxide species on a Ti site [31,32,34,35,60]. In the case of propane oxidation, a similar set of steps is likely, with propane probably reacting with a hydroperoxide species to form an 2-propoxy intermediate [11,13]. This species can readily desorb to form 2-propanol or undergo further oxidation with $H_2O_2$ to produce acetone [11,13,62].

The likely sequence of steps for propane oxidation can be deduced from a combination of in situ spectroscopic techniques and kinetic measurements. In the case of $H_2$ oxidation and propylene epoxidation with $H_2$ and $O_2$ on gold catalysts, significant advances have been realized through in situ UV–vis and XAFS spectroscopic techniques [30,33,34] augmented by density functional theory (DFT) calculations [35]; for example, for propylene epoxidation, Ti-hydroperoxo species recently was found to be a true intermediate by means of transient in situ XANES spectroscopy [34]. In the case of propane oxidation, recent evidence for adsorption and activation of $O_2$ on Au has been provided in an $Au/TiO_2$ catalyst by in situ UV–vis and XANES spectroscopy [10] as well as in an Au–Ba/TS-1 catalyst by in situ UV–vis spectroscopy [11]. In situ UV–vis spectroscopy also has provided evidence for the formation of Ti-hydroperoxo and tripodal Ti(OH) sites in a Au–Ba/TS-1 catalyst [11]. The present study provides additional evidence in support of the presence of adsorbed $O_2$ on Au and the formation of Ti(OOH) and Ti(OH) sites, and proof that Ti(OOH) species is a true reaction intermediate.

In situ UV–vis spectra of Au/TS-1 as a function of reaction time during propane oxidation conditions demonstrated noticeable changes in three main regions: (1) a band at about 520 nm (2.38 eV) due to a plasmon resonance (PR) of Au nanoparticles; (2) a band increase at 350 nm (3.54 eV), assigned to hydrated Ti(OOH) species; and (3) a band increase at 240 nm (5.17 eV), assigned to tripodal Ti(OH) sites (see Supporting Information). The Au PR feature was symmetric, indicating that the gold particles had a regular shape and a relatively narrow size distribution, consistent with the TEM results (Fig. 1) [63,64]. Tracking of the Au PR position as a function of reaction time provided additional information regarding the adsorptive properties of the Au nanoparticles (Fig. 5). The Au PR position shifted toward higher wavelengths (red shift) initially (in the first 0.5 h), but then moved toward lower wavelengths (blue shift) thereafter, reaching an almost constant value after about 2 h of reaction. The initial red shift of the Au PR was due to $O_2$ adsorption on Au and can be explained by the lower density of free electrons in the gold as a result of charge transfer from the surface metal atoms to adsorbed $O_2$ [42,43]. The subsequent blue shift possibly occurred because the adsorbed $O_2$ on Au reacted with $H_2$ as steady conditions were reached. Some adsorbed $O_2$ remained, as suggested by the higher Au PR position (520.3 nm) compared with that observed for the catalyst under reductive $H_2$ flow (516.0 nm), which served as the source of the steady production of the hydroperoxide species. The in situ UV–vis difference spectra in Fig. 6 show the simultaneous formation of hydrated $Ti(OOH)(H_2O)_2$ (355 nm) and tripodal $Ti(OOH)(OSi)_3$ (237 nm) sites more clearly. A shoulder at around 272 nm is likely related to hydrated tripodal $Ti(OH)(OSi)_3$ [41]. The TS-1 (Ti/Si = 3/100) support has isolated tetrahedral $Ti(OSi)_4$ sites incorporated in the framework of a crystalline silica zeolite (structure type MFI) [12,17,41,48]. These tetrahedral $Ti(OSi)_4$ sites can be readily transformed by hydrolysis into tripodal $Ti(OH)(OSi)_3$ sites, as supported by theoretical calculations [65]. The participation of this $Ti(OH)(OSi)_3$ site in hydrocarbon oxidation with $H_2O_2$ also has been suggested recently based on theoretical calculations [66,67]. The small increase in the Ti(OOH) signal over 5 h corresponds to the small increase in conversion over the same time period (Fig. 2). This is likely due

to a secondary effect involving the Ti centers, which are somewhat distant from the Au particles. The Au particles first supply $H_2O_2$ to neighboring Ti centers, which are responsible for the first immediate reaction products, but as supply and demand for $H_2O_2$ becomes balanced for those sites, the more distant centers come into play.

In the absence of separate experiments to determine absolute coverages, proving that these observed species are true intermediates and not spectators is not possible with UV–vis spectroscopy alone. Later in the paper, we use in situ Ti *K*-edge XANES measurements to demonstrate that Ti(OOH) is a true intermediate species during propane oxidation.

Gold particles were found in the vicinity of Ti, although not necessarily bonded directly to the tetrahedral Ti sites [29]. The in situ Au $L_3$-edge XANES results for Au/TS-1 showed that the Au in the catalyst was mostly metallic (Fig. 7), and that the presence of oxidized Au, characterized by a near-edge resonance of ca. 11,920 eV (e.g., $HAuCl_4$), was not observed. In situ Au $L_3$-edge XANES difference spectra, $\mu$(Reaction) $-\mu$(He, at 443 K before reaction) (Fig. 8), showed the evolution of a near-edge transient resonance (white line) at about 11,921 eV during the first 0.1 h of reaction, which later decreased to reach a near-stable value after 1.0–1.5 h of reaction. The intensity of this white line in the Au $L_3$-edge arises from unoccupied d-states; therefore, interactions between adsorbed molecules and gold clusters should have an effect on this resonance [44,45]. The initial increase in intensity of the white line can be related to the chemisorption of $O_2$ on Au particles (Au–O complex formation) as the d-orbital electron count of gold is decreased by charge transfer to the $2\pi^*$ orbital of $O_2$ [44,45]. The subsequent decrease in intensity of the white line as the reaction reaches a near-steady value corresponds to a reduction of the Au–O complex (in the air-calcined sample) by reaction with $H_2$. This behavior is similar to that observed for propane oxidative dehydrogenation with $H_2$ and $O_2$ on $Au/TiO_2$ catalysts, which showed an initial increase of the Au $L_3$-edge white line, followed by a decrease due to reduction of the Au–O complex with $H_2$ [10]. Similar trends were also found for a 4 wt% $Au/Al_2O_3$ catalyst subsequently exposed to $O_2$ and CO [45]. The Au $L_3$-edge white line exhibited an increase in intensity during $O_2$ exposure, followed by a decrease due to reaction of the formed Au–O complex with CO to produce $CO_2$. Overall, the in situ Au $L_3$-edge XANES difference spectra results are in line with Au PR measurements under reaction conditions, which also indicates initial adsorption of $O_2$ on Au and its further reaction with $H_2$ to likely form hydroperoxide species.

We used a previously reported transient technique to identify reaction intermediates [34]. The technique involves measuring the initial transient coverage changes ($d\theta/dt$) on fourfold-coordinated Ti as determined from intensity changes in the Ti pre-edge peak centered at about 4968.9 eV in the in situ Ti *K*-edge XANES spectra using two different reacting environments: a $H_2/O_2/He = 1/1/8$ gas mixture, which corresponds to hydroperoxide species synthesis conditions, and a $H_2/O_2/C_3H_8/He = 1/1/1/7$ gas mixture, which corresponds to propane oxidation conditions. The net reaction of the hydroperoxide species includes its formation ($r_{for}$) and decomposition rates ($r_{decomp}$):

$$(d\theta/dt)_{synthesis} = r_{for} - r_{decomp},$$

whereas the net reaction of propane oxidation includes not only hydroperoxide species formation ($r_{for}$) and decomposition rates ($r_{decomp}$), but also the reaction rate to form oxygenates from propane ($r_{oxid}$),

$$(d\theta/dt)_{oxid} = r_{for} - r_{decomp} - r_{oxid}.$$

The net rate of oxidation was calculated as the difference between the two slopes,

$$r_{oxid} = (d\theta/dt)_{synthesis} - (d\theta/dt)_{oxid}.$$

The method described here assumes that measurements of the changes in the pre-edge peak intensity of the Ti *K*-edge region are indicative of adsorption. This assumption is reasonable, because the pre-edge peak is characteristic of the tetrahedral geometry on the Ti sites before adsorption, and changes in coordination result in extinction of the peak intensity [47]. It also assumes that the step involving the reaction of the Ti hydroperoxide species is a slow step in the reaction, which is consistent with the kinetic results, as we discuss later.

The pre-edge peak in the Ti *K*-edge XANES spectra for Au/TS-1 centered at 4969.0 eV is a salient feature; see Fig. 9. This pre-edge peak arises from the normally symmetry forbidden 1s→3d transition because of mixing of sp-states in tetrahedrally coordinated Ti (Ti(Td)), and it provides a wealth of information regarding the Ti oxidation state and local geometry [46,47,68,69]. Under propane oxidation conditions with the standard $H_2/O_2/C_3H_8/He = 1/1/1/7$ mixture, a simultaneous decrease in the Ti pre-edge normalized absorption and increase in the intensity of the feature at 4985.5 eV indicates the formation of higher-coordinated Ti species as a result of adsorption. Similar results were obtained for the in situ Ti *K*-edge XANES measurements with the $H_2/O_2/He = 1/1/8$ mixture and are not shown for the sake of brevity. The fractional decrease in the Ti pre-edge area from its value before the introduction of reactants is defined as the coverage on the Ti(Td) centers, $\theta$. Fig. 10 shows the coverage on fourfold-coordinated Ti for Au/TS-1 under $H_2/O_2/C_3H_8/He = 1/1/1/7$ and $H_2/O_2/He = 1/1/8$ mixtures. Following the method described earlier, the initial net rate of propane oxidation based on Ti coverage, $\theta$, is estimated as $6.7 \times 10^{-4}$ $s^{-1}$ (Fig. 10). This value is similar to the TOF for propane oxidation to oxygenates at steady-state of $5.6 \times 10^{-4}$ $s^{-1}$ based on total Ti (Table 1, run *S*), indicating that the Ti-hydroperoxide species is a true intermediate in the gas-phase oxidation of propane with $H_2$ and $O_2$. Comparing the initial transient rate by XANES to the steady-state rate is justified because the Ti sites are isolated, and thus interactions are not expected.

A possible simplified sequence of steps for propane oxidation with $H_2$ and $O_2$ on Au/TS-1 consistent with the kinetic results, the in situ spectroscopic study, and previously reported observations is as follows:

$$O_2 + * \rightleftarrows O_2^* \quad (1)$$

$$H_2 + 2\bullet \rightleftarrows 2H\bullet \quad (2)$$

$$O_2^* + H\bullet \rightleftarrows HOO^* + \bullet \quad (3)$$

$$HOO^* + H_2 + \bullet \rightarrow H_2O_2 + * + H\bullet \quad (4)$$

$$H_2O_2 + Ti(OH) \rightleftarrows Ti(OH)(HOOH) \quad (5)$$

$$Ti(OH)(HOOH) \rightleftarrows Ti(OH_2)(OOH) \quad (6)$$

$$Ti(OH_2)(OOH) + CH_3CH_2CH_3 \rightleftarrows Ti(OH_2)(OOH)(HCH(CH_3)_2) \quad (7)$$

$$Ti(OH_2)(OOH)(HCH(CH_3)_2) \rightarrow Ti(OH_2)(OCH(CH_3)_2) + H_2O \quad (8)$$

$$Ti(OH_2)(OCH(CH_3)_2) \rightleftarrows Ti(OH) + CH_3CH(OH)CH_3 \quad (9)$$

$$Ti(OH_2)(OCH(CH_3)_2) + H_2O_2 \longrightarrow Ti(OH) + 2H_2O + CH_3COCH_3 \quad (10)$$

The first part of this reaction sequence (steps (1)–(4)) involves the formation of $H_2O_2$ on two types of Au sites (∗ and •), as suggested by previous studies of $H_2$ oxidation and propylene epoxidation with $H_2$ and $O_2$ [31,32,35,60]. The second part of the reaction sequence (steps (5)–(8)) involves the formation of Ti-hydroperoxide species from tetrahedral Ti sites and $H_2O_2$ [66,67],

which then react with propane to produce a 2-propoxy intermediate species [11,13]. This 2-propoxy species can then form 2-propanol (step (9)) or acetone (step (10)) [13,62]. Assuming that steps (4) (formation of $H_2O_2$) and (8) (formation of 2-propoxy species) are slow steps, that $H_2O_2$ can decompose to $H_2O$ via a parallel first-order pathway, and that the rate of formation of the 2-propoxy species (step (8)) mostly determines the rate of formation of oxygenates, we can derive a power-rate law expression of the form $r_{oxyg.} = k_{oxyg.}(H_2)^k(O_2)^l(C_3H_8)^m$ based on the foregoing sequence of steps. As shown elsewhere, the derivation of a rate expression for a similar sequence of steps in propylene epoxidation with $H_2$ and $O_2$ on a Au–Ba/Ti-TUD catalyst [31,32] allows us to solve the following set of equations simultaneously to provide a final expression:

- From steps (1) to (4),

$$r_{H_2O_2} = \frac{\alpha(O_2)(H_2)^{3/2}}{[1+\beta(O_2)+\gamma(O_2)(H_2)^{1/2}][1+\delta(H_2)^{1/2}]}, \tag{11}$$

  where $\alpha$, $\beta$, $\gamma$, and $\delta$ are constant quantities resulting from combinations of the total number of Au adsorption sites for $H_2$ ($\bullet$) and $O_2$ ($*$) and reaction rate coefficients of steps (1) to (4).
- From steps (5) to (8),

$$r_{oxyg.} = \frac{\kappa(H_2O_2)(C_3H_8)}{[1+\lambda(H_2O_2)+\mu(H_2O_2)(C_3H_8)]}, \tag{12}$$

  where $\kappa$, $\lambda$, and $\mu$ are also constant quantities resulting from combinations of the total number of Ti(OH) adsorption sites and reaction rate coefficients of steps (5) to (8).
- Finally, accounting for a first-order decomposition of $H_2O_2$,

$$r_{H_2O_2} = r_{oxyg.} + r_{decomp} = r_{oxyg.} + k_D(H_2O_2). \tag{13}$$

The foregoing set of equations can be further simplified by assuming that in the denominator of (12), the term $\lambda(H_2O_2) + \mu(H_2O_2)(C_3H_8)$ may be $<1$ if $H_2O_2$ concentrations are relatively low, resulting in

$$r_{oxyg.} \approx \kappa(H_2O_2)(C_3H_8). \tag{14}$$

Solving (11), (13), and (14) simultaneously yields

$$r_{oxyg.} = \frac{\alpha(O_2)(H_2)(H_2)^{1/2}}{[1+\beta(O_2)+\gamma(O_2)(H_2)^{1/2}][1+\delta(H_2)^{1/2}]} \times \frac{(C_3H_8)}{[k_D/\kappa+(C_3H_8)]}. \tag{15}$$

The left-side term of (15) is similar to the rate of formation of $H_2O$ from $H_2$ and $O_2$ on Au catalysts reported earlier [35]. Assuming that $\delta(H_2)^{1/2} > 1$, it will cancel the $(H_2)^{1/2}$ in the numerator. The final result is an expression of the form $r_{oxyg.} = k_{oxyg.}(H_2)^k(O_2)^l(C_3H_8)^m$, where the order for $H_2$ is between 0.5 and 1 and the orders for $O_2$ and $C_3H_8$ are between 0 and 1, which correspond well with the respective power-rate fitting results of 0.74, 0.36, and 0.29. Overall, the suggested reaction pathway is in close agreement with these kinetic results and the spectroscopic observations of activation of oxygen on gold, as well as the formation of reactive hydroperoxide species on Ti, and provides a good description of the reaction of propane oxidation on Au/TS-1. Additional support for this model comes from the fact that it provides a better fit to the reaction data than the generic power-rate law equation (see Supporting Information). Our kinetic and spectroscopic results can be used to provide support for a mechanism involving the reaction of hydroperoxide species with propane to form oxygenates.

## 5. Conclusion

This work demonstrated the efficient production of oxygenates (acetone and 2-propanol) from propane, $H_2$, and $O_2$ on a 0.52 wt% Au/TS-1 (Ti/Si = 3/100) catalyst at 443 K and 0.1 MPa. The combined selectivity for oxygenates was always >90%, with acetone (75–93%) as the main product, followed by 2-propanol (4–19%) and then $CO_2$ (1–6%). We studied the reaction using kinetic and spectroscopic techniques. The rate of formation of oxygenates is well described by a power-rate model of the form $r_{oxyg.} = k_{oxyg.}(H_2)^{0.74}(O_2)^{0.36}(C_3H_8)^{0.29}$. Apparent activation energies for the formation of $H_2O$, acetone, and $CO_2$ were 42, 38, and 40 kJ mol$^{-1}$, respectively. In situ Au $L_3$-edge XANES and UV–vis spectroscopy under reaction conditions demonstrated the formation of $O_2$ adsorbed on Au, which may react with $H_2$ to form hydroperoxide species. Ti-hydroperoxo species were detected by in situ UV–vis spectroscopy and were demonstrated to be true intermediates by a transient Ti *K*-edge XANES technique. A possible sequence of steps has been proposed: (1) $H_2O_2$ is formed from $H_2$ and $O_2$ on gold; (2) $H_2O_2$ is transferred to Ti centers to form Ti-hydroperoxo species; (3) Ti-hydroperoxo species react with propane to form 2-propoxy intermediate species; and (4) 2-propoxy species form acetone and 2-propanol. The proposed reaction pathway produced a rate of formation of oxygenates consistent with the experimental power-rate law kinetic results.

## Acknowledgments

The authors acknowledge financial support from the Ministry of Economy, Trade and Industry (Minimum Energy Chemistry project) and the National Science Foundation (CBET 0651238). Financial support also was provided by the Japan Society for the Promotion of Science through the postdoctoral fellowship for foreign researcher program (P05627, to J.J.B.-S.) and the invited fellow program (to S.T.O.). The authors thank Ms. E. Kobayashi and Dr. K. Kawasaki for the TEM measurements. The XAFS experiments were conducted under the approval of PF-PAC (proposals 2004G304 and 2006G362).

## Supplementary material

The online version of this article contains additional supplementary material.

Please visit DOI: 10.1016/j.jcat.2008.04.004.

## References

[1] M. Haruta, Catal. Today 36 (1997) 153.
[2] M. Haruta, Cattech 6 (2002) 102.
[3] A.S.K. Hashmi, G.J. Hutchings, Angew. Chem. Int. Ed. 45 (2006) 7896.
[4] M.D. Hughes, Y.-J. Xu, P. Jenkins, P. McMorn, P. Landon, D.I. Enache, A.F. Carley, G.A. Attard, G.J. Hutchings, F. King, E.H Stitt, P. Johnston, K. Griffin, C.J. Kiely, Nature 437 (2005) 1132.
[5] D.I. Enache, J.K. Edwards, P. Landon, B. Solsona-Espriu, A.F. Carley, A.A. Herzing, M. Watanabe, C.J. Kiely, D.W. Knight, G.J. Hutchings, Science 311 (2006) 362.
[6] M. Haruta, N. Yamada, T. Kobayashi, S. Iijima, J. Catal. 115 (1989) 301.
[7] G.R. Bamwenda, S. Tsubota, T. Nakamura, M. Haruta, Catal. Lett. 44 (1997) 83.
[8] T. Hayashi, K. Tanaka, M. Haruta, Prep.-Am. Chem. Soc., Div. Pet. Chem. 41 (1996) 71.
[9] T. Hayashi, K. Tanaka, M. Haruta, J. Catal. 178 (1998) 566.
[10] J.J. Bravo-Suárez, K.K. Bando, J.Q. Lu, T. Fujitani, S.T. Oyama, J. Catal. 255 (2008) 114.
[11] J.J. Bravo-Suárez, K.K. Bando, T. Fujitani, S.T. Oyama, Chem. Commun. (2008), in press.
[12] M. Taramasso, G. Perego, B. Notari (Enichem), US Patent 4,410,501 (1983).
[13] C.B. Khouw, C.B. Dartt, J.A. Labinger, M.E. Davis, J. Catal. 149 (1994) 195.
[14] M.G. Clerici, Appl. Catal. 68 (1991) 249.
[15] M.G. Clerici, P. Ingallina, Catal. Today 41 (1998) 351.
[16] D.R.C. Huybrechts, L. De Bruycker, P.A. Jacobs, Nature 345 (1990) 240.
[17] B. Notari, Adv. Catal. 41 (1996) 253.

[18] R. Murugavel, H.W. Roesky, Angew. Chem. Int. Ed. 36 (1997) 477.
[19] W.L. Howard, Acetone, Kirk Othmer Encyclopedia of Chemical Technology, Wiley & Sons, 2002.
[20] R.J. Schmidt, Appl. Catal., A 280 (2005) 89.
[21] Z.-C. He, Xiandai Huagong/Mod. Chem. Ind. 25 (11) (2005) 61.
[22] G.I. Panov, Cattech 4 (2000) 18.
[23] P.P. Notté, Top. Catal. 13 (2000) 387.
[24] New Technology, Benzene-to-phenol process ready for commercialization, Focus Catal. (2004) 6.
[25] P. Paredes Olivera, E.M. Patrito, H. Sellers, Surf. Sci. 313 (1994) 25.
[26] M. Okumura, Y. Kitagawa, K. Yamaguchi, T. Akita, S. Tsubota, M. Haruta, Chem. Lett. 32 (2003) 822.
[27] A. Corma, M. Boronat, S. González, F. Illas, Chem. Commun. (2007) 3371.
[28] N. Yap, R.P. Andres, W.N. Delgass, J. Catal. 226 (2004) 156.
[29] B. Taylor, J. Lauterbach, W.N. Delgass, Appl. Catal., A 291 (2005) 188.
[30] B. Chowdhury, J.J. Bravo-Suárez, M. Daté, S. Tsubota, M. Haruta, Angew. Chem. Int. Ed. 45 (2006) 412.
[31] J.Q. Lu, X. Zhang, J.J. Bravo-Suárez, S. Tsubota, J. Gaudet, S.T. Oyama, Catal. Today 123 (2007) 189.
[32] J.J. Bravo-Suárez, J.Q. Lu, C.G. Dallos, T. Fujitani, S.T. Oyama, J. Phys. Chem. C 111 (2007) 17427.
[33] B. Chowdhury, J.J. Bravo-Suárez, N. Mimura, J.Q. Lu, K.K. Bando, S. Tsubota, M. Haruta, J. Phys. Chem. B 110 (2006) 22995.
[34] J.J. Bravo-Suárez, K.K. Bando, J.Q. Lu, M. Haruta, T. Fujitani, S.T. Oyama, J. Phys. Chem. C 112 (2008) 1115.
[35] D.G. Barton, S.G. Podkolzin, J. Phys. Chem. B 109 (2005) 2262.
[36] R.B. Khomane, B.D. Kulkarni, A. Paraskar, S.R. Sainkar, Mater. Chem. Phys. 76 (2002) 99.
[37] NIST/SEMATECH e-Handbook of Statistical Methods, http://www.itl.nist.gov/div898/handbook/ (accessed Feb. 06, 2007), Section 5.3.3.10.
[38] M. Shacham, M.B. Cutlip, M. Elly, Polymath, Copyright 2006.
[39] H.S. Fogler, Elements of Chemical Reaction Engineering, third ed., Prentice–Hall PTR, Upper Saddle River, NJ, 2006.
[40] G. Kortüm, Reflectance Spectroscopy, Springer, Berlin, 1969.
[41] P. Ratnasamy, D. Srinivas, H. Knözinger, Adv. Catal. 48 (2004) 1.
[42] W. Cai, H. Hofmeister, T. Rainer, Physica E 11 (2001) 339.
[43] W. Cai, H. Hofmeister, T. Rainer, W. Chen, J. Nanopart. Res. 3 (2001) 443.
[44] N. Weiher, A.M. Beesley, N. Tsapatsaris, L. Delannoy, C. Louis, J.A. Van Bokhoven, S.L.M. Schroeder, J. Am. Chem. Soc. 129 (2007) 2240.
[45] J.A. Van Bokhoven, C. Louis, J.T. Miller, M. Tromp, O.V. Safonova, P. Glatzel, Angew. Chem. Int. Ed. 45 (2005) 4651.
[46] M. Fernández-García, Catal. Rev. 44 (2002) 59.
[47] F. Farges, G.E. Brown Jr., J.J. Rehr, Phys. Rev. B 56 (1997) 1809.
[48] G.N. Vayssilov, Catal. Rev.—Sci. Eng. 39 (1997) 209.
[49] K. Tamaru, Dynamic Heterogeneous Catalysis, Academic Press, New York, 1978.
[50] C. Reed, Y. Xi, S.T. Oyama, J. Catal. 235 (2005) 378.
[51] S.T. Oyama, W. Li, Top. Catal. 8 (1999) 75.
[52] I. Yamanaka, S. Hasegawa, K. Otsuka, Appl. Catal., A 226 (2002) 305.
[53] C. Espro, F. Arena, F. Tasselli, A. Regina, E. Drioli, A. Parmeliana, Catal. Today 118 (2006) 253.
[54] E.E. Stangland, K.B. Stavens, R.P. Andres, W.N. Delgass, J. Catal. 191 (2000) 332.
[55] C. Sivadinarayana, T.V. Choudhary, L.L. Daemen, J. Eckert, D.W. Goodman, J. Am. Chem. Soc. 126 (2004) 38.
[56] V.N. Shetti, P. Manikandan, D. Srinivas, P. Ratnasamy, J. Catal. 216 (2003) 461.
[57] M.A. Vannice, Kinetics of Catalytic Reactions, Springer, New York, 2005.
[58] G. Djéga-Mariadassou, M. Boudart, J. Catal. 216 (2003) 89.
[59] K. Ruth, M. Hayes, R. Burch, S. Tsubota, M. Haruta, Appl. Catal., B 24 (2000) L133.
[60] B. Taylor, J. Lauterbach, G.E. Blau, W.N. Delgass, J. Catal. 242 (2006) 142.
[61] T.A. Nijhuis, B.M. Weckhuysen, Catal. Today 117 (2006) 84.
[62] J.E. Rekoske, M.A. Barteau, J. Catal. 165 (1997) 57.
[63] U. Kreibig, M. Vollmer, Optical Properties of Metal Clusters, Springer, Berlin, 1995.
[64] L.M. Liz-Marzán, Langmuir 22 (2006) 32.
[65] P.E. Sinclair, G. Sankar, C.R.A. Catlow, J.M. Thomas, T. Maschmeyer, J. Phys. Chem. B 101 (1997) 4232.
[66] R.R. Sever, T.W. Root, J. Phys. Chem. B 107 (2003) 4080.
[67] D.H. Wells Jr., W.N. Delgass, K.T. Thomson, J. Am. Chem. Soc. 126 (2004) 2956.
[68] F.M.F. de Groot, A. Knop-Gericke, T. Ressler, J.A. van Bokhoven, in: B.M. Weckhuysen (Ed.), In-situ Spectroscopy of Catalysts, American Scientific Publishers, Stevenson Ranch, CA, 2004, p. 107.
[69] J.M. Thomas, G. Sankar, Acc. Chem. Res. 34 (2001) 571.